JOURNAL OF MATERIALS SCIENCE 29 (1994) 6273–6280

Solubility, reactivity and nucleation effect of Cr_2O_3 in the CaO–MgO–Al_2O_3–SiO_2 glassy system

L. BARBIERI, C. LEONELLI, T. MANFREDINI, G. C. PELLACANI, C. SILIGARDI
Department of Chemistry, Via Campi 183, 41100 Modena, Italy

E. TONDELLO, R. BERTONCELLO
Department of Inorganic, Metallorganic and Analytical Chemistry, Via Loredan 4, 35131 Padova, Italy

The effect of Cr_2O_3 on some anorthite–diopside glass-ceramics has been investigated up to amounts of 5 mol%. The solubility in the glassy compositions analysed is total for the oxide, but for amounts higher than 0.5 mol%, an insoluble spinel form, $MgCr_2O_4$, precipitates. Ultraviolet–visible spectroscopy has proved to be the most sensitive technique to the presence of Cr(III) in a crystalline spinel site, followed by X-ray diffraction and scanning electron microscopy observations. Electron spin resonance and X-ray photoelectron spectroscopy techniques excluded any oxidation state, other than Cr^{3+}. The influence of the transition cation on glass nucleation is that of an increasing bulk effect with chromium, and thus chromium–spinel, content. The magnesium content affects spinel formation, while heat treatments up to 1100 °C do not. The spinel formation influences the anorthite–diopside ratio in the glass-ceramic, with a large favour towards the pyroxene.

1. Introduction

Chromium, being a transition metal ion, shows a particularly mobile 3d electronshell, which favours variable valence states, from divalent to hexavalent, and coordination numbers, four and six in the oxide, making it a very efficient colouring agent in glasses. In colouring glasses, chromium has been usually found to prevail in the most stable trivalent oxidation state [1].

A further interest in chromium oxides from a theoretical and a practical point of view derives from the fact that Cr_2O_3 is also a very effective additive for controlling the rate of nucleation in many glasses. Depending on the concentration, it can have various roles: (a) it may increase homogeneous nucleation rate by increasing the bulk free-energy change upon crystallization, by reducing the crystal–liquid interfacial free energy or by increasing the diffusion rate; (b) alternatively, it may precipitate, in combination with other components in the glass, and initiate heterogeneous nucleation of a major phase [2, 3]. In particular, Cr_2O_3 has a great tendency to form spinel-like compounds with other oxides, such as MgO, FeO, Fe_2O_3 and Al_2O_3, which, precipitating as a high density of fine crystals, act as heterogeneous sites for glass crystallization [4, 5].

We previously investigated [6, 7] the glass to glass-ceramic transformation of two surface-nucleated glassy compositions, belonging to the quaternary CaO–MgO–Al_2O_3–SiO_2 system, which gave diopside ($CaO \cdot MgO \cdot 2SiO_2$) and anorthite ($CaO \cdot Al_2O_3 \cdot 2SiO_2$) crystals in 3:1 and 1:1 ratio, respectively. The effect of crystallization catalysts upon crystal nucleation, stable phases and solid solutions is particularly important for imparting certain properties to the glass-ceramic products. In this paper we report a thermal, microscopic, diffractometric and spectroscopic study on the effect of Cr_2O_3 added to the above system in place of identical amounts of CaO (0.2, 0.5, 0.7, 1.0, 1.5, 5.0 mol%) with the aim to identify the influence of the transition metal cation on nucleation and crystallization mechanisms, to describe the local surroundings of the chromium atom in the glassy and glass-ceramic network, and to determine the oxidation states of the transition metal cation.

Further interest derives from the fact that, in recent studies [8–10], it has been demonstrated that Cr_2O_3 has a catalytic effect on the pyroxene crystallization of a glass in the CaO–MgO–Al_2O_3–SiO_2 (CMAS) system, where the major crystal phase is diopside.

2. Experimental procedure

2.1. Sample preparation

All the investigated compositions (Table I) belong to two different base compositions in the quaternary CaO–MgO–Al_2O_3–SiO_2 system, corresponding to the following molar fractions $0.25CaO–0.20MgO–0.05Al_2O_3–0.50SiO_2$ (A) and $0.25CaO–0.14MgO–0.11Al_2O_3–0.50SiO_2$ (B), which, on heat treatment,

0022–2461

TABLE I Molar composition, heat treatments and crystalline phases of the studied materials (magnesium-chromite, $MgO \cdot Cr_2O_3$, JCPDS 10-351; diopside, $CaO \cdot MgO \cdot 2SiO_2$, JCPDS 11-654; anorthite, $CaO \cdot Al_2O_3 \cdot 2SiO_2$, JCPDS 12-301)

Name	Composition (mol %)					Heat treat. (°C, h)	Crystalline phases
	Cr_2O_3	CaO	MgO	Al_2O_3	SiO_2		
A		25.031	19.725	5.146	50.098	–	None
						1100, 1	Diopside, anorthite (tr.)
ACr0.2	0.2	24.831	19.725	5.146	50.098	–	None
						1100, 1	Diopside, anorthite (tr.)
ACr0.5	0.5	24.531	19.725	5.146	50.098	–	None
						1100, 1	Diopside, anorthite (tr.)
ACr0.7	0.7	24.331	19.725	5.146	50.098	–	Mg-chromite (tr.)
						1100, 1	Diop., Mg-chrom., an.(tr.)
ACr1.5	1.5	23.531	19.725	5.146	50.098	–	Mg-chromite
						1100, 1	Diop., Mg-chrom., an.(tr.)
ACr5	5	20.531	19.725	5.146	50.098	–	Mg-chromite
						900, 48	Mg-chromite
						1000, 24	Diop., Mg-chrom.
						1100, 1	Diop., Mg-chrom., an.(tr.)
B		25.031	13.972	10.931	50.066	–	None
						1100, 1	Diopside, anorthite
BCr0.2	0.2	24.831	13.972	10.931	50.066	–	None
						1100, 1	Diopside, anorthite
BCr0.5	0.5	24.531	13.972	10.931	50.066	–	None
						1100, 1	Diopside, anorthite
BCr0.7	0.7	24.331	13.972	10.931	50.066	–	Mg-chromite (tr.)
						1100, 1	Diop., Mg-chrom., an.
BCr1.5	1.5	23.531	13.972	10.931	50.066	–	Mg-chromite
						1100, 1	Diop., Mg-chrom., an.(tr.)
BCr5	5	20.531	13.972	10.931	50.066	–	Mg-chromite
						900, 48	Mg-chromite
						1000, 24	Diop., Mg-chrom.
						1100, 1	Diop., Mg-chrom., an.(tr.)

give glass-ceramics containing anorthite and diopside in 1:3 and 1:1 ratios, respectively. In these systems, 0.2, 0.5, 0.7, 1.0, 1.5 and 5.0 mol % CaO were substituted with identical amounts of Cr_2O_3. The chromium(III)-containing raw materials were in the form of reagent-grade nitrate.

The raw materials were melted in platinum crucibles in an electric furnace at 1400 °C and immediately quenched in water to obtain amorphous material. All the Cr_2O_3-doped glassy samples were transparent up to 0.5 mol % dopant. The remaining glasses, which were not completely transparent because of the solubility limit of Cr_2O_3, were re-melted at 1400 °C for 3 h. After such a period of time it could be assumed that the maximum solubility of Cr_2O_3 in the amorphous matrix was reached, while the excess chromium was present as spinel crystallite.

Heat treatment of glasses was carried out in a single stage in an electrical furnace at different temperatures and soaking times (Table I) for both the colourless and doped samples. As a consequence of the heating, the doped samples darkened to a varying extent and became more greyish, depending both on Cr_2O_3 and MgO concentration.

2.2. Thermal measurements

Differential thermal analysis was performed with a Netzsch STA 409 thermobalance, to 1400 °C on ground, as-melted, glassy frits with different particle sizes. DTA curves were automatically recorded at different heating rates. A blank run with 20 mg calcined kaolin as reference material was performed over the same temperature range used in the DTA runs.

2.3. Microstructural analyses

Microstructural studies were performed on freshly fractured specimens of glassy and glass-ceramic samples with an optical microscope and scanning electron microscope, SEM (Philips PSEM 500). An approximate chemical analysis of each different phase of the materials was also determined using energy dispersive analysis of X-rays (EDX, EDAX PV 9900).

Diffractometric measurements of powdered glass-ceramic samples of particle size dimensions $< 20\ \mu m$ were collected with an X-ray (nickel-filtered CuK_α, $\lambda = 0.15418$ nm) powder diffractometer (Philips PW 1050) with a 2 s time constant and 1000 counts range in the 2θ range from 10°–45° at a scanning rate of $1° \min^{-1}$. Repeated experiments proved the reproducibility of the results. The X-ray diffraction patterns were interpreted using ASTM diffraction files and the crystalline phases obtained are indicated in Table I.

2.4. Spectroscopic measurements

Spectroscopic measurements were performed on powdered samples of all the doped glasses and glass-ceramics having particle size distribution $< 20\ \mu m$.

Electronic absorption spectra were measured on a spectrophotometer (Cecil 6000) working in the 300–800 nm range. Samples were spread on a strip of paper and were measured against a strip of paper as blank.

Room-temperature electron spin resonance (ESR) measurements were run using the X-band (9.76 GHz) of a spectrometer (Varian E-9). Polycrystalline DPPH was used as a standard g-marker ($g = 2.0036$).

X-ray photoelectron spectra (XPS) were recorded in a spectrometer (VG Escalab MK II) using non-monochromatized AlK_α radiation (1486.6 eV) at 13 kV with a current of 20 mA on samples containing 5 mol % dopant. The spectrometer was calibrated by assuming the binding energy (BE) of the Au $4f_{7/2}$ line at 83.9 eV with respect to the Fermi level. Samples exhibit an average shift of about 14 eV due to surface charging. The 1s photoelectron from carbon, from hydrocarbon contamination ($E = 284.80$ eV [11]), was used as an internal reference for the charging effects. XPS spectra were carried out on pellets obtained by pressing powdered samples. The reproducibility of results was assured by repeated experiments on the same pellet.

3. Results and discussion

For each composition, the Cr_2O_3 (see Table I) was mixed with the powder batch before the first melting. Substitution for Ca^{2+} rather than Mg^{2+}, was done because (a) the six-fold coordinated site of Mg^{2+} cation in diopside can be substituted with cations of similar ionic radii, ranging from 0.053–0.083 nm, such as Fe(III), Mn(II) and Cr(III) (as an example $NaCrSi_2O_6$), (b) Mg^{2+} plays a fundamental role in the spinel formation, and (c), probably as a consequence of the first two points, Mg^{2+} is a constituent of the crystalline form, calcium(II) magnesium(II) pyroxene (diopside), on which Cr_2O_3 has been found to exert a catalytic effect.

3.1. As-quenched glasses

3.1.1. Microstructural results

SEM observation on the fresh fractured glassy samples revealed the presence of some crystallite in all the composition where the solubility limit of Cr_2O_3 (about 0.5 mol %) was exceeded. As an example, a scanning electron micrograph of the glassy BCr0.5 sample is shown in Fig. 1. Crystals of dimension 2–5 μm are observed, which are proved by means of a qualitative EDS analysis to contain magnesium and chromium. Particles of the unreacted chromium oxide have not been found in any of the Cr_2O_3-doped samples.

X-ray powder diffractometric measurements (Fig. 2) have been performed on the glassy samples in order to identify the chemical nature of the crystallites observed above. All the compositions containing Cr_2O_3 up to about 0.5 mol % show XRD patterns characteristic of the glassy state, with no indication of crystalline phases. When the Cr_2O_3 concentration exceeds 0.5 mol %, a crystalline phase is observed, for which the major peaks correspond to magnesium chromite

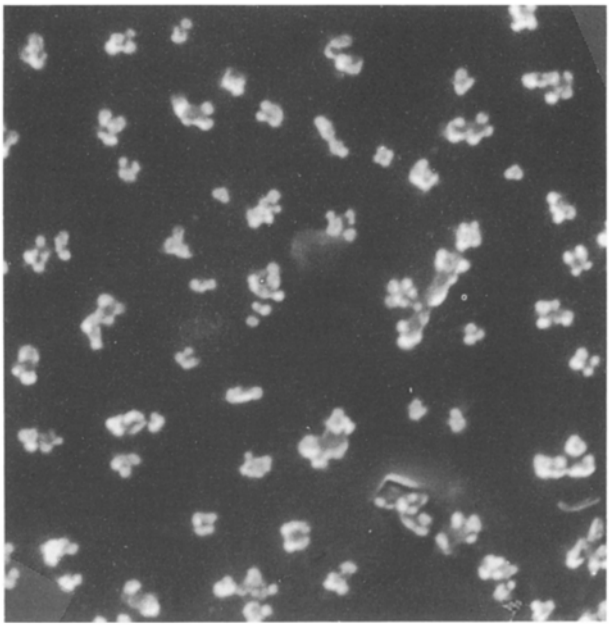

Figure 1 Scanning electron micrograph of glass BCr0.5 freshly fractured surface, × 4000 mag.

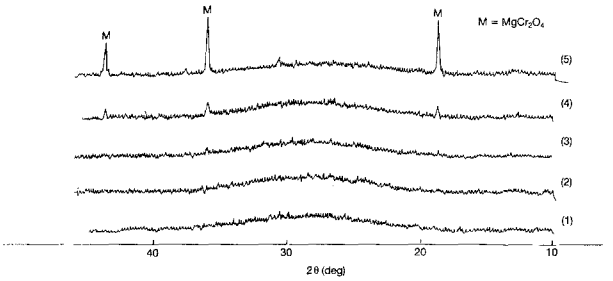

Figure 2 XRD patterns on as-quenched glasses of composition (1) ACr0.2; (2) ACr0.5; (3) ACr0.7; (4) ACr1.5; (5) ACr5.

spinel $MgCr_2O_4$ (JCPDS 10-351) and the concentration of which varies directly with the Cr_2O_3 content. Increasing the chromium–spinel content results in an increase in the peak intensity and sharpness (Fig. 2).

The high reactivity of the chromium(III) oxide with the base CMAS system is demonstrated, because no Cr_2O_3 crystals were identified in the glassy specimens, even when the fusion temperature was held for longer than 1 h. By reaction of Cr_2O_3 with MgO at the melting temperature of the glass, the spinel of formula $MgO \cdot Cr_2O_3$ is formed. The bulk reaction can be represented as follows

$$[Cr_2O_3] + (MgO) = \{MgCr_2O_4\} \quad (1)$$

where [ ] refers to solid solution species in the specimens, ( ) refers to a species dissolved in the melt, and { } refers to a solid solution species in the spinel reaction product. A slight dependence on the MgO content can be observed in Fig. 3 where the absolute peak intensity of the highest spinel ($d = 0.251$ nm) diffraction are reported for the two compositions, ACr5 and BCr5, as a function of reaction time at 1400 °C. The spinel content is higher for A compositions and is time-independent.

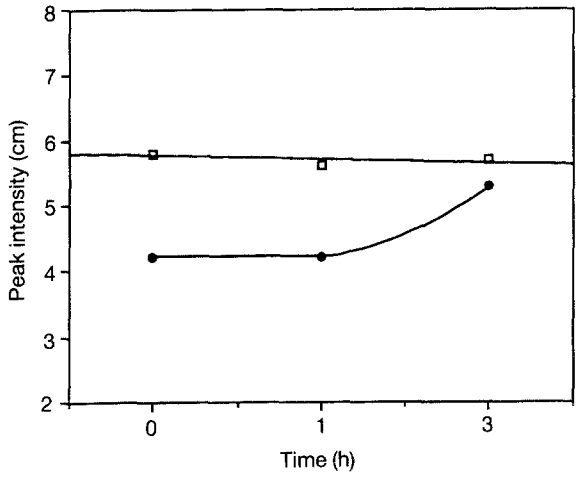

Figure 3 Peak intensity of 0.250 nm diffraction for Cr–spinel crystal dependence on fusion soaking time: (●) BCr5, (□) ACr-5.

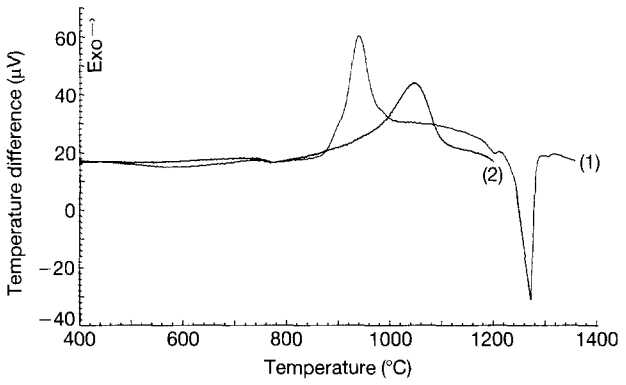

Figure 4 DTA curves for BCr0.2 glasses at 10 °C min^{-1} heating rate with (1) < 20 μm and (2) 0.5 mm grain size.

3.1.2. Thermal analysis

The DTA data were collected on different particle-sized samples from compositions ACr0.2, BCr0.2, ACr5, and BCr5 in order to observe the influence of Cr^{3+} when present exclusively inside the glassy matrix, as in the 0.2 mol % chromium-containing samples, and also in spinel crystallites, as when 5 mol % dopant is used.

Fig. 4 shows the DTA curves for different particle sizes of BCr0.2 glass. When the grain size is increased from 20 μm to 500 μm the shift of the crystallization peak temperature, T_c, is 70–100 °C for 0.2 mol % dopant. The doped A and B composition glasses react very similarly in DTA, presenting a typical thermal behaviour of an easily devitrifiable glass. After the change in slope due to the glass transition, T_g, an exothermic peak for the crystallization is visible. The highest temperature peak represents the endothermic fusion. A shift of the crystallization peak maximum temperature, T_c, towards higher temperature, compared to the colourless base specimens, is noted even in the case of 0.2 mol % Cr_2O_3 (Table II). The dopant effect was similar on T_g. Omar *et al.* observed the same effect on T_c [12].

A shoulder of the crystallization peak on the low-temperature side, is relevant for fine powders (< 20 μm). Both the appearance of the shoulder and the T_c shift due to grain size lead to the conclusion that there is a double nucleation mechanism: (1) a bulk nucleation which prevails when the dimensions of the glassy grains and chromium content are large (500 μm) and (2) a secondary surface nucleated mechanism for finest (20 μm) powders and smallest dopant content.

Activation energies for the crystallization process were determined only from DTA curves run on 20 μm powders of compositions ACr0.2, ACr5, BCr0.2, BCr5 (Table II). The mathematical approach used for this study was the Kissinger method described by Matusita–Sakka [13, 14]. The basis of this method was the relationship between heating rate and exothermic peak temperature

$$-\,\mathrm{d}[\ln(\Phi^n/T_c^2)]/\mathrm{d}[1/T_c] \;=\; -\,mE_{ck}/R \qquad (2)$$

where Φ is the heating rate (2, 5, 10 K min^{-1}) of the DTA run, T_c (K) is the exothermic peak temperature maximum, R the gas constant (1.9872 cal mol^{-1} K^{-1}), E_{ck} the activation energy for crystallization (cal/mol), and n and m are numerical constants which depend on the crystallization mechanism which should previously be known. Compared to the undoped glass the activation energy values for composition A-doped glasses appear to decrease with chromium content, while an opposite trend is visible for B composition.

The values of n and m have been evaluated according to Xu *et al.* [15] (Table II) and with some approximation it could be observed that $n = m = 1$ for every composition. This result suggests that for fine pow-

TABLE II Crystallization peak temperatures at different heating rates, in alumina crucibles, and activation energies for the studied compositions (r = correlation coefficient)

Heating rate (°C min^{-1})	T_c(°C)					
	A	ACr0.2	ACr5	B	BCr0.2	BCr5
2	890	896	901	904	895	920
5	912	925	924	922	920	942
10	930	939	938	934	940	976
20	944	950	946	956	947	985
n	1	1	0.61	1	1.68	1.24
m	1	0.87	1.44	1	0.7	0.46
E_{ck} (kcal mol^{-1})	113	113	135	124	112	91
r	0.998	0.983	0.986	0.992	0.982	0.978

ders, even at 5 mol % chromium content, the surface nucleation mechanism is prevalent.

The dimensionality of crystalline growth for glasses with a grain size of about 500 μm was found to be around $m = 2$, confirming the observation on peak shapes reported above, the study of Omar *et al.* [12] and Robson and Davies [10].

3.2. Glass-ceramics

3.2.1. XRD on crystallized glasses

The glassy samples were treated in a muffle furnace at 1100 °C for 1 h, after which no residual glass was observed. Two common crystalline phases, diopside and anorthite, were found for both compositions A and B, while the spinel phase, $MgCr_2O_4$, was present in those samples with a chromium oxide concentration higher than 0.2 mol % (Fig. 5). For soaking times of 3 h at 1100 °C no increase in the amount of chromium-spinel was ever noticed, so it can be deduced that the formation of magnesium chromite has been completed during the fusion step.

Interesting results have been achieved with longer heat treatment at lower temperature (1000 °C for 24 h). In glasses having composition B, considerable amounts of Cr_2O_3 catalysed the process of crystallization of diopside, and inhibited anorthite phase growth (Fig. 6). For A compositions, characterized by a lower anorthite content, the effect of chromium was detected mainly as an increase of diopside peak sharpness. The formation of chromium–spinel crystallite, $Mg(Al, Cr)_2O_4$, in this glass system was suggested and so was the tendency to favour diopside formation observed by Omar *et al.* [12]. The present observations suggest this is mainly a thermodynamic effect rather than a kinetic one.

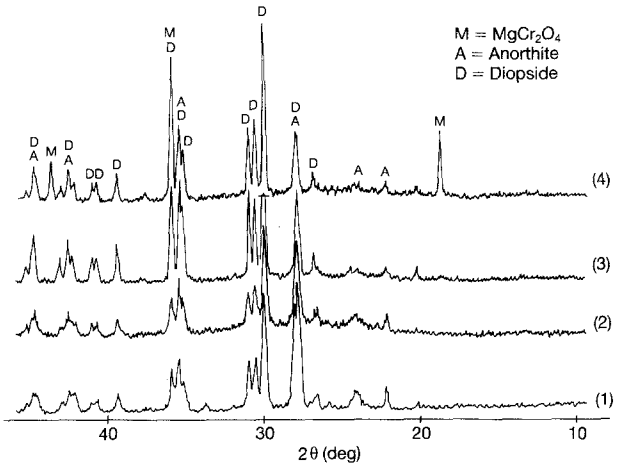

Figure 5 XRD patterns on glass-ceramics treated at 1100 °C for 1 h of compositions (1) B, (2) BCr0.2; (3) BCr0.7; (4) BCr5.

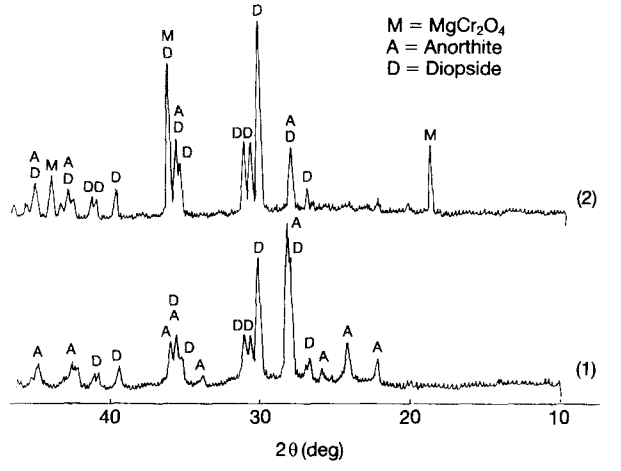

Figure 6 XRD patterns of glass-ceramics treated at 1000 °C for 24 h of compositions (1) B and (2) BCr5.

3.2.2. Glass-ceramic microstructure

SEM observations (Fig. 7) on fresh fractured large glass-ceramic pieces of both compositions revealed that heat treatment (1100 °C, 1 h) promoted a random crystalline growth, mostly bulk nucleated while in the undoped samples the surface nucleation mechanism was much more evident with its crystal growth direction from the outside to the inside of the piece [6].

3.3. UV–VIS spectra

The glassy samples present a colour from clear to deep green, depending on the chromium(III) oxide concentration, which remains after crystallization. The same bands were observed in the spectra of all glass and glass-ceramic samples, for both compositions A and B (Figs 8 and 9).

When dopant addition to the glass is less than 0.5 mol %, the absorption bands appear at 440 and 650 nm, which are consistent with Cr^{3+} in an octahedral environment. The bands are assigned on the basis of Durville *et al.*'s observations [16] to $3d \rightleftharpoons 3d$ electron transition, but the hyperfine structure is not visible in the presented spectra. The low-energy tail of the 650 nm peak shows that Cr^{3+} ions remain in glassy state.

For addition of Cr_2O_3 higher than 0.5 mol %, a new band appears at 560 nm, characteristic of Cr^{3+} in the octahedral site of the pure spinel $MgCr_2O_4$ [17–19], which presents a line at 550 nm.

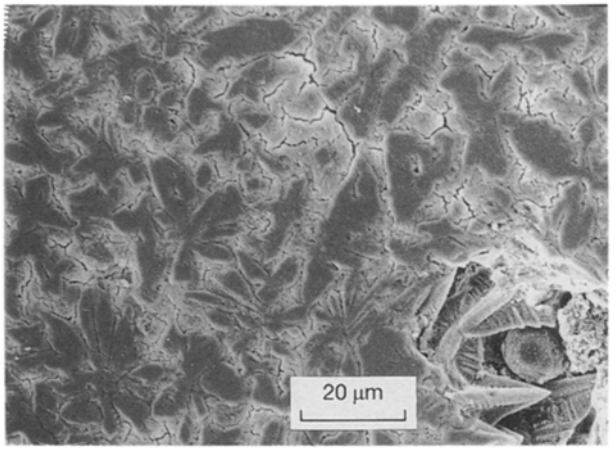

Figure 7 Scanning electron micrograph of BCr0.7 glass-ceramics treated at 1000 °C for 1 h; polished and etched surface.

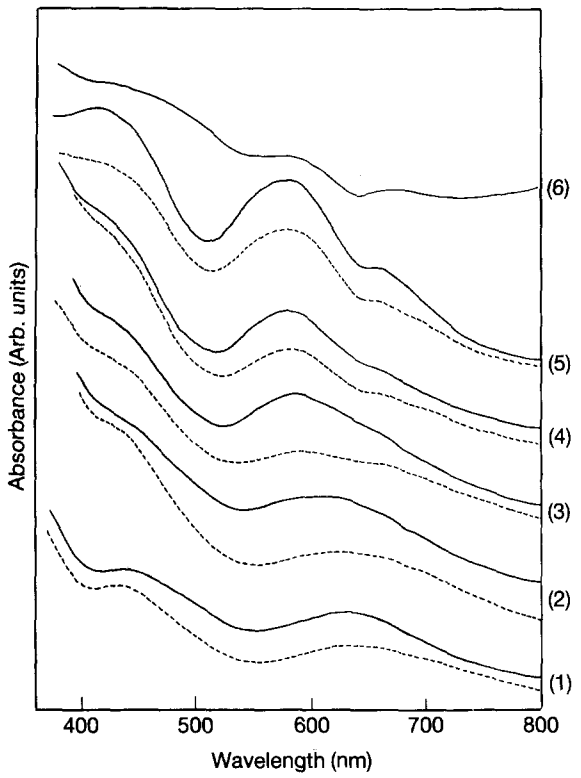

Figure 8 UV–VIS spectra in the 400–800 nm range of (···) glass and (——) glass-ceramic samples of compositions (1) ACr0.2, (2) ACr0.5, (3) ACr0.7, (4) ACr1.5, (5) ACr5, compared to that of (6) pure magnesium chromite.

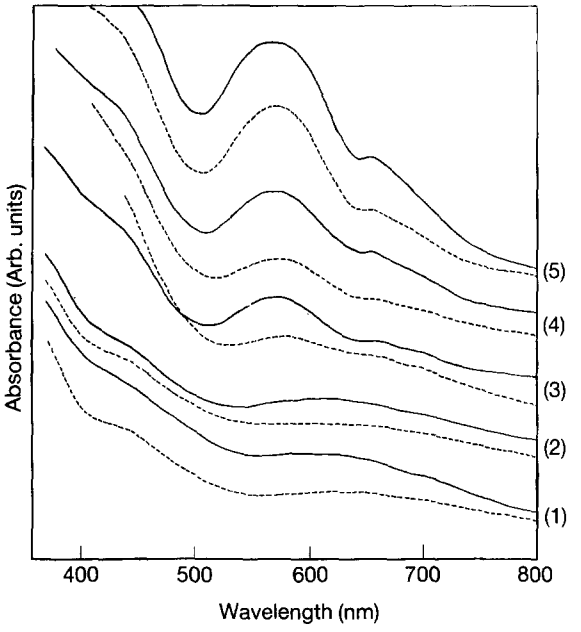

Figure 9 UV–VIS spectra in the 400–800 nm range of (···) glass and (——) glass-ceramic samples of compositions (1) BCr0.2, (2) BCr0.5, (3) BCr0.7, (4) BCr1.5, (5) BCr5.

The absorption bands of Cr^{3+} in the crystalline state in the observable $^4A_2 \rightarrow {}^4T_2$ transition are shifted to higher energy as compared with the glassy state. The oscillator strength in the crystalline phase is generally lower by a factor of 2 compared to the glassy phase. This is not surprising because in the glassy state, Cr^{3+} resides in a symmetry lower than in the crystalline state, thus enhancing parity-forbidden $3d \rightleftharpoons 3d$ transition.

For glass at a high concentration of Cr_2O_3, detail of the absorption bands at high energies (Fig. 10) shows the weak signal at 340 nm, which corresponds either to a very low amount of Cr^{6+} or to an effect due to the glass matrix [19].

These observations in the UV–VIS spectral range proved that the coordination of Cr^{3+} in the glass matrix and in the spinel is the same, but the symmetry is distorted, indicating the growth of the spinel inside an amorphous material containing more than 0.5 mol % of dopant. The spinel presence is related even to the increased absorption at 400 nm, for the glasses at higher chromium content.

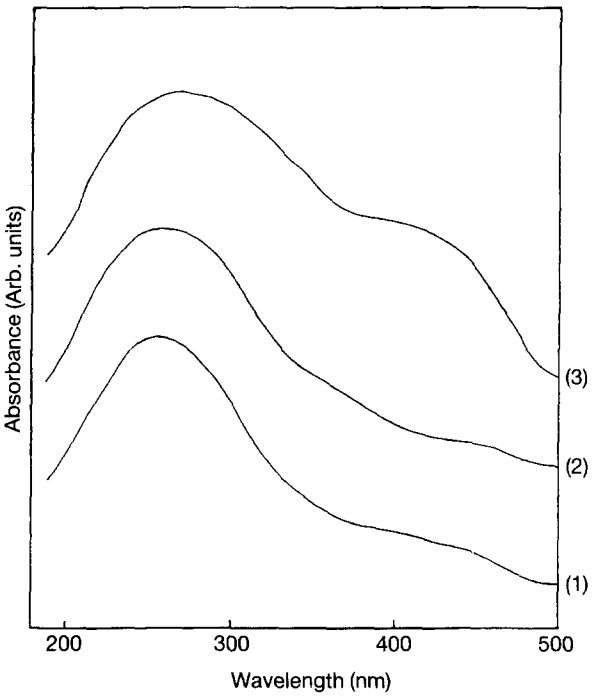

Figure 10 UV–VIS spectra in the 200–600 nm range of glasses of compositions (1) B, (2) BCr0.2, (3) BCr5.

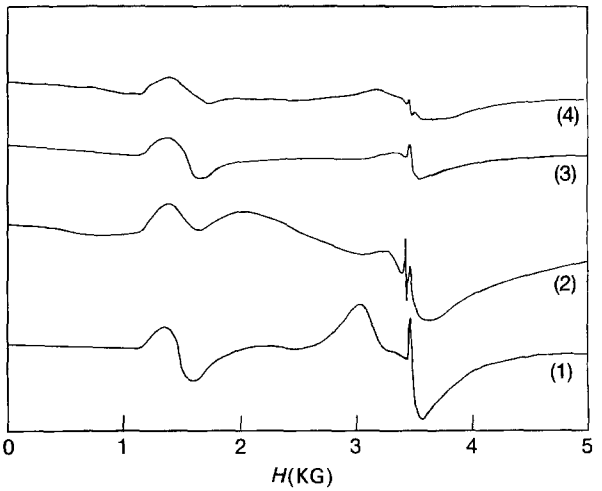

Figure 11 ESR spectra at room temperature of samples (1) ACr0.2 glass, (2) ACr0.2 glass-ceramic, (3) BCr0.2 glass, and (4) BCr0.2 glass-ceramic.

3.4. ESR spectra

The ESR spectra for 0.2 and 0.5 mol % Cr_2O_3-containing samples showed similar features (Figs 11 and 12). The signal centred at $g_{eff} = 5.5$ is typical of Cr^{3+} ions in the glassy sites, octahedral symmetry with rhombic distortion [8, 20]. The broad resonance signal $g_{eff} = 1.95$ was attributed to Cr^{3+} ions by previous investigations [8, 20–22]. This last signal is characteristic of Cr^{3+} ions strongly coupled by antiferromagnetic exchange interactions and magnetic dipolar interactions ([16] and references therein cited). This signal broadens in the glass-ceramic samples, indicating that Cr^{3+} ions diffuse and concentrate in some points, inducing some kind of nucleation. This signal, together with the presence of the absorption band at 560 nm, was also attributed by Durville *et al.* [16] to the Cr^{3+} ion in a trigonal site of the $Mg(Al_{1-x}Cr_x)_2O_4$ spinel, with x close to 1.

The spectra were characterized also by a sharp signal at $g_{eff} = 1.97$, which decreases from glassy to the crystallized state, and which was attributed by different authors [8, 20–22] to small amounts of Cr^{5+}, in the octahedral site with tetragonal distortion.

3.5. XPS spectra

XPS measurements have been performed on powdered glasses and glass-ceramics from A composition doped with 5 mol % Cr_2O_3 (3.6% atomic abundance) in order to obtain appreciable results.

XPS spectroscopy showed the presence of only one oxidation form, Cr(III). The $2p_{3/2}$ and $2p_{1/2}$ peaks of Cr^{3+} appear at binding energy values of 576.6 and 586.3 eV, respectively [23]. The $2p_{3/2}$ peak width (fwhm = 3.0 eV, experimental) is comparable with that for samples of pure Cr_2O_3 (fwhm = 3.125 eV, theoretical) such as to exclude the presence of Cr^{6+}, in the form of CrO_3, which should present a $2p_{3/2}$ peak at a binding energy of 578.1 eV with a consequent broadening of the Cr(III) peak.

No differences have been noticed between the two spectra of glassy samples melted at 1400 °C for 1 h and for 3 h. No evidence of Cr(VI) was found. The presence of relevable quantity of Cr(VI) is thus not correlated with melting time in these compositions, as suggested by Omar *et al.* [9]. Also passing from the glass to the glass-ceramic there is no evidence of the presence of a different oxidation state other than Cr(III).

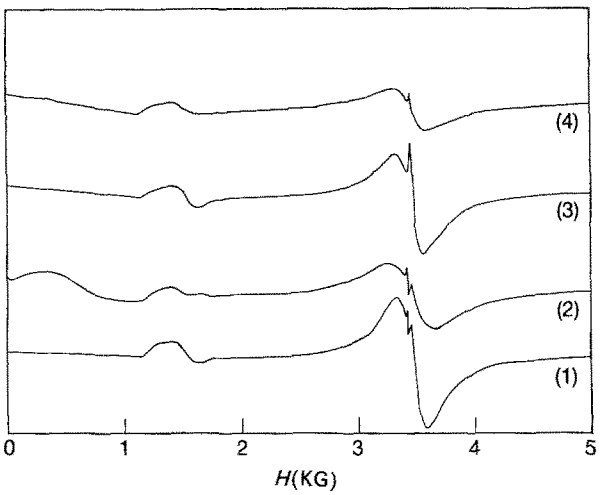

Figure 12 ESR spectra at room temperature of samples (1) ACr0.5 glass, (2) ACr0.5 glass-ceramic, (3) BCr0.5 glass, and (4) BCr0.5 glass-ceramic.

4. Conclusions

The relative amount of spinel in comparison to the other crystalline forms, anorthite and diopside, is time-dependent at 1400 °C for composition B and becomes time and temperature-independent for both compositions at lower temperatures. The spinel presence in the glass influences the nucleation mechanism, which is partially transformed from surface-activated to bulk-initated. This effect is particularly evident at high Cr_2O_3 content.

The crystalline structure of the magnesium-chromite is such as to favour diopside growth, especially for long-term heat treatments. The glass or glass-ceramic matrix do not affect the chromium oxidation state, + 3, which always presents an octahedral symmetry with little distortion, when present in the spinel site, and is present in amounts of Cr(V) in the glassy samples at low chromium content.

Acknowledgements

The authors thank Professor F. Cariati and Dr S. Bruni, Inorganic and Metallorganic Chemistry Department, Milan University, for their helpful ESR discussion, and MURST for financial support.

References

1. M. B. VOLF, "Chemical Approach to Glass", "Glass Science and Technology", Vol. 7 (Elsevier, Amsterdam, 1984) pp. 334–9.
2. G. H. BEALL and D. A. DUKE, in "Glass-Ceramic Technology", "Glass: Science and Technology", Vol. 1, edited by D. R. Uhlmann and N. J. Kreidl (Academic Press, New York, 1983) pp. 886–99.
3. P. F. JAMES, in "Volume nucleation in silicate glasses", "Glasses and Glass-ceramics", edited by M. H. Lewis (Chapman and Hall, London, 1989) pp. 61–105.
4. F. DURVILLE, B. CHAMPAGNON, E. DUVAL, F. GAUME, A. F. WRIGHT and A. N. FITCH, *Phys. Chem. Glasses* **25** (1984) 126.
5. H. S. KIM, R. D. RAWLINGS and P. S. ROGERS, *J. Mater. Sci.* **24** (1989) 1025, and references quoted therein.
6. C. LEONELLI, T. MANFREDINI, M. PAGANELLI, P. POZZI and G. C. PELLACANI, *ibid.* **26** (1991) 5041.
7. L. BARBIERI, C. LEONELLI, T. MANFREDINI, M. PAGANELLI and G. C. PELLACANI, *J. Thermal Anal.* **38** (1992) 2639.
8. S. DINGKUN and L. A. ORLOVA, *J. Non-Cryst. Solids* **112** (1989) 207.
9. A. A. OMAR, A. W. A. El-SHENNAWI and G. A. KHATER, *Br. Ceram. Trans. J.* **90** (1991) 179, and references quoted therein.
10. M. J. ROBSON and M. W. DAVIES, BISRA-C/64/69 (1971).
11. M. P. SEAH and G. C. SMITH, in "Practical Surface Analysis", edited by D. Briggs and M. P. Seah, Vol. 1, 2nd Edn, Appendix 1 (Wiley, Chichester, 1990) pp. 543–4.
12. A. A. OMAR, S. M. SALMAN and M. Y. MAHMOUD, *Ceram.* **15** (1985) 57, and references quoted therein.
13. K. MATUSITA, S. SAKKA and Y. MATSUI, *J. Mater. Sci.* **10** (1975) 961.

14. K. METUSITA and S. SAKKOR, *J. Non-Cryst. Solids* **38–39** (1980) 741.
15. X. J. XU, C. S. RAY and D. F. DAY, *J. Am. Ceram. Soc.* **74** (1991) 909.
16. F. DURVILLE, B. CHAMPAGNON, E. DUVAL and G. BOULON, *J. Phys. Chem. Solids* **46** (1985) 701.
17. R. REISFELD, A. KISILEV, E. GREENBERG, A. BUCH and M. ISH-SHALOM, *Chem. Phys. Lett.* **104** (1984) 153.
18. *Idem, ibid.* **105** (1984) 405.
19. P. C. SCHULTZ, *J. Am. Ceram. Soc.* **57** (1974) 178.
20. D. E. O'REILLY and D. S. Mac IVER, *J. Phys. Chem.* **66** (1962) 276.
21. K. TANAKA and K. KIMIYA, *J. Mater. Sci. Lett.* **10** (1991) 1095.
22. D. L. GRISCOM, *J. Non-Cryst. Solids* **40** (1980) 211.
23. C. D. WAGNER, W. M. RIGGS, L. E. DAVIS, J. S. MOULDER and G. E. MUILNBERD, in "Handbook of X-ray Photoelectron Spectroscopy", edited by C. D. Wagner (Perkin Elmer, Eden Prairie, USA, 1978).

Received 13 May 1993
and accepted 27 May 1994